

Projective Quantum Eigensolver via Adiabatically Decoupled Subsystem Evolution: a Resource Efficient Approach to Molecular Energetics in Noisy Quantum Computers

Chayan Patra,¹ Sonaldeep Halder,¹ and Rahul Maitra^{1, 2, a)}

¹⁾Department of Chemistry,

Indian Institute of Technology Bombay,
Powai, Mumbai 400076, India

²⁾Centre of Excellence in Quantum Information, Computing, Science & Technology,
Indian Institute of Technology Bombay,
Powai, Mumbai 400076, India

Quantum computers hold immense potential in the field of chemistry, ushering new frontiers to solve complex many body problems that are beyond the reach of classical computers. However, noise in the current quantum hardware limits their applicability to large chemical systems. This work encompasses the development of a projective formalism that aims to compute ground-state energies of molecular systems accurately using Noisy Intermediate Scale Quantum (NISQ) hardware in a resource efficient manner. Our approach is reliant upon the formulation of a bipartitely decoupled parameterized ansatz within the disentangled unitary coupled cluster (dUCC) framework based on the principles of *synergetics*. Such decoupling emulates the total parameter optimization in a lower dimensional manifold, while a mutual synergistic relationship among the parameters is exploited to ensure characteristic accuracy. Without any *pre-circuit measurements*, our method leads to a highly compact fixed-depth ansatz with shallower circuits and fewer expectation value evaluations. Through analytical and numerical demonstrations, we demonstrate the method's superior performance under noise while concurrently ensuring requisite accuracy in future fault-tolerant systems. This approach enables rapid exploration of emerging chemical spaces by efficient utilization of near-term quantum hardware resources.

I. INTRODUCTION

The exact description of many body systems evolve in an exponentially growing Hilbert space (with system size), leading to eventually an intractable problem¹ and restricting the conventional computers to rely heavily on mean-field approaches for real-life applications. However, these mean-field approaches often inherently ignore the important physics, such as the correlation effects within an ensemble of interacting particles. For atomic and molecular systems, these electron-electron correlation effects are of paramount importance in chemistry and condensed matter physics and are taken care of by theories like density matrix renormalization group (DMRG)², selected configuration interaction^{3,4} and different variants of the coupled cluster (CC) methods^{5–9}. Despite being able to predict the energies accurately, these methods have an exponential or higher-order polynomial cost, hindering their usage for most of the practical applications.

Quantum computers hold great promise in the field of electronic structure theory, particularly for simulating the electronic behavior of molecules and materials. Such platforms leverage principles of superposition and entanglement to store and manipulate many-fermion wavefunctions. Early quantum algorithms, including those employing Quantum Phase Estimation (QPE)^{10,11}, played a pioneering role in this domain. However, these methods rely on deep quantum circuits, which may surpass the coherence times available in current quantum

hardware^{12–14}. Additionally, these quantum devices suffer from poor gate fidelity, state preparation and measurement errors (SPAM), and readout errors. As a result, computations performed using deep quantum circuits are prone to significant inaccuracies. To overcome these challenges, methods have been developed that require comparatively shallower circuits and have inherent noise resilience. Variational Quantum Eigensolver¹⁵ (VQE) is one such method that conforms to the limitations of the current noisy quantum hardware. It prepares a parameterized state within the quantum computing framework using a shallow depth circuit (ansatz). The optimum parameters are obtained through classical variational minimization of the energy expectation value. Several other variants^{16–30} of VQE framework have been proposed to further minimize the ansatz depth. Another promising method, the Projective Quantum Eigensolver (PQE)^{31–33} also relies on generating a parameterized quantum state where the parameters are optimized by solving a set of nonlinear projective equations. This method is also shown to exhibit inherent noise resilience and has a faster convergence (specifically under noise) as compared to VQE³¹. Moreover, it does not show the barren plateau problem^{34,35}, often encountered during variational energy minimization in the VQE framework. PQE can be used with disentangled unitary coupled cluster ansatz (dUCC)³⁶, which is capable of capturing a substantial amount of correlation energy of molecular systems. When coupled with a CNOT efficient implementation^{37,38}, dUCC offers a flexible and efficient ansatz structure for application in molecular systems.

Nevertheless, when dealing with large and highly cor-

^{a)}Electronic mail: rmaitra@chem.iitb.ac.in

related molecules, implementing dUCC demands deep quantum circuits and a large number of optimizable parameters. While increased depth leads to large errors in computed energetics for practical applications, more parameters require many quantum measurements during the PQE iterative method. Hence, there is a pressing need to develop methods capable of overcoming these challenges to attain accurate molecular energetics within the limited coherence time of noisy quantum hardware.

In this work, we have developed a “two-phase” formalism in the PQE framework with the aim of reducing the quantum resources (*both* circuit gate depth and measurements) utilized during the non-linear iterative optimization. The approach is based on the judicious partitioning of the PQE parameter space into a smaller dimensional *principal* parameter subspace and a larger dimensional *auxiliary* subspace. The authors had previously substantiated that these two subspaces have distinctly different timescales of equilibration, allowing us to adiabatically decouple^{39–41} the fast relaxing *auxiliary* modes from the slow relaxing *principal* modes^{42–49}. Consequently, *auxiliary* parameters can be expressed as a mathematical function of the principal parameters that projects the parameter optimization in a lower dimensional manifold. This is popularly known in literature as the *slaving principle*^{50–56}. We use this decoupling paradigm within the PQE non-linear optimization scheme and analytically establish the function that maps elements of *auxiliary* space from the *principal* one. Taking a step further, we introduce a *no-feedback-control* formalism, where we capture the effective dependence of the *auxiliary* parameters on the *principal* ones through a one-step *post-optimization mapping*. This allows us to perform PQE within the lower dimensional and fully disjoint *principal* subspace. Previous studies⁴⁷ focusing on subspace decoupling within the PQE formalism showed promise but depended on machine learning and assumed an ideal, noise-free quantum device. Additionally, the approach only resulted in measurement reduction. Other dimensionality reduction techniques such as the subsystem embedding subalgebra coupled cluster (SES-CC)^{57,58} and their quantum computing counterpart^{59–61} have also been previously explored, but they operate on different underlying principles. This manuscript delineates the first attempt to formulate and demonstrate the effectiveness of an analytic adiabatic subspace decoupling to come up with an optimally resource-efficient quantum algorithm toward realistic implementation under hardware noise.

Our approach serves twin desirable goals – while allowing us to perform PQE with a fixed structured shallow circuit, it also markedly reduces measurement costs during optimization. This becomes even more advantageous on noisy quantum devices as the reduction in the circuit depth entails less noise and shows better effectiveness towards various error mitigation strategies. Moreover, the compactification of the ansatz does not involve any pre-circuit measurement (measurements prior to the construction of the final ansatz circuit). Thus, the

structural optimality of the ansatz is not deteriorated by noise. Molecular energy calculations on NISQ hardware are typically noise-dominated rather than correlation-dominated. As a consequence, significantly shallower circuits, though seemingly accurate on NISQ devices, might not fully capture electronic correlation due to insufficient parameterization. This limitation is likely to become more apparent as the noise in quantum hardware is reduced. The hallmark of a robust ansatz is thus its ability to balance expressibility and agility under noise. In this regard, an open and nontrivial question that we numerically address in this manuscript is the choice of the optimal dimension for the principal subspace that balances the two opposing effects, such that the theory which is reasonably accurate in the NISQ era can also be seamlessly adopted when better hardware becomes available. This flexibility enables our method to be used under various hardware infrastructures with varying degrees of noise, facilitating the exploration of upcoming emerging chemical phenomena in a hardware-agnostic way.

The manuscript is structured as follows: we begin by formalizing the *no-feedback-controlled* adiabatically decoupled PQE (*nfcAD-PQE*). Following this, we present a mathematical foundation establishing its resource efficiency and utility in noisy quantum hardware. Subsequently, we demonstrate its efficiency and accuracy in an ideal, noiseless scenario. In the final section, we illustrate the efficacy of *nfcAD-PQE* under noise and compare it with conventional PQE.

II. THEORETICAL DEVELOPMENT OF NO-FEEDBACK-CONTROLLED ADIABATICALLY DECOUPLED PROJECTIVE QUANTUM EIGENSOLVER

A. Emergence of Collective Behaviour: Slaving Principle in Projection Based Unitary Coupled Cluster Theory

Projective Quantum Eigensolver (PQE)³¹ relies on the preparation of a parameterized trial wavefunction $|\Psi(\theta)\rangle$ by the action of a unitary $\hat{U}(\theta)$ on a reference state $|\Phi_o\rangle$, often taken to be the Hartree Fock (HF) state

$$|\Psi(\theta)\rangle = \hat{U}(\theta) |\Phi_o\rangle \quad (1)$$

Here, in the disentangled Unitary Coupled Cluster (dUCC) ansatz³⁶, \hat{U} is taken to be -

$$\hat{U}(\theta) = \prod_{\mu} e^{\theta_{\mu} \hat{\kappa}_{\mu}} \quad (2)$$

where, $\hat{\kappa}_{\mu} = \hat{\tau}_{\mu} - \hat{\tau}_{\mu}^{\dagger}$ is an anti-Hermitian operator with $\hat{\tau}_{\mu} = \hat{a}_a^{\dagger} \hat{a}_b^{\dagger} \dots \hat{a}_j \hat{a}_i$. In the above equations, μ represents a multi-index particle-hole excitation structure as defined by the string of creation (\hat{a}^{\dagger}) and annihilation (\hat{a}) operators with the indices $\{i, j, \dots\}$ denoting the occupied

spin-orbitals in the HF state and $\{a, b, \dots\}$ denoting the unoccupied spin-orbitals.

PQE determines the optimal parameters by considering it as a nonlinear optimization problem, which is accomplished iteratively via residue construction-

$$\theta_\mu^{(k+1)} = \theta_\mu^{(k)} + \frac{r_\mu^{(k)}}{D_\mu}. \quad (3)$$

where, k represents an iterative step with D_μ denoting the second-order Moller Plesset (MP2) denominator. The residue (r_μ) is obtained by projecting the Schrodinger equation against excited determinants $\{|\Phi_\mu\rangle\}$ -

$$r_\mu(\boldsymbol{\theta}) = \langle \Phi_\mu | \hat{U}^\dagger(\boldsymbol{\theta}) H \hat{U}(\boldsymbol{\theta}) | \Phi_o \rangle; \mu \neq 0 \quad (4)$$

r_μ can be executed on a quantum computer as a sum of three expectation value calculations³¹-

$$r_\mu = \langle \Omega_\mu(\pi/4) | \bar{H} | \Omega_\mu(\pi/4) \rangle - \frac{1}{2} E_\mu - \frac{1}{2} E_0 \quad (5)$$

with the following definitions, $|\Omega_\mu(\theta)\rangle = e^{\hat{\kappa}_\mu \theta} |\Phi_0\rangle$, $\bar{H} = \hat{U}^\dagger \hat{H} \hat{U}$, $E_\mu = \langle \Phi_\mu | \bar{H} | \Phi_\mu \rangle$ and $E_0 = \langle \Phi_0 | \bar{H} | \Phi_0 \rangle$. The iterative procedure is deemed converged when

$$r_\mu(\boldsymbol{\theta}^*) \rightarrow 0 \text{ (at fixed point } \boldsymbol{\theta}^*) \quad (6)$$

However, in examining the discrete-time iteration dynamics (Eq. (3)), a discernible hierarchical structure emerges regarding the convergence timescale. Notably, parameters of larger magnitudes require a significantly larger number of iterations to achieve convergence compared to their smaller magnitude counterparts⁴⁷. In general, for a certain class of multivariable nonlinearly coupled dynamical systems, such co-existing hierarchy among the components can be exploited to eliminate the fast-decaying variables. This method projects the system in a lower dimensional manifold in the phase space that indeed simplifies the complex motion to a great extent. For a mathematical analysis, let us cast the parameter update equation in a generic discrete-time dynamical form by reordering Eq. (3) and expanding the residual vector r_μ into linear and nonlinear parts-

$$\Delta\theta_\mu = \Lambda_\mu \theta_\mu + M(\{\theta\}) \quad (7)$$

where, Δ is a *difference operator* in a discretized time domain such that $\Delta\theta_\mu = \theta_\mu^{(k+1)} - \theta_\mu^{(k)}$, Λ_μ is the coefficient of the diagonal linear term and $M(\{\theta\})$ encapsulates the off-diagonal linear terms and all nonlinear couplings among the parameters. For a qualitative phase-space analysis of such a nonlinear system, one can perturb the system slightly from a fixed point and perform a *linear stability analysis*^{42,62} that divides the variables into two parts based on the following conditions on the eigen values (λ) of the *stability matrix*

$$\begin{aligned} \{\lambda_P\} < 0; & \text{ corresponds to slow eigendirections: principal modes (total number } N_P) \\ \{\lambda_A\} < 0; & \text{ corresponds to fast eigendirections: auxiliary modes (total number } N_A) \end{aligned} \quad (8)$$

with the very important condition:

$$|\lambda_A| > |\lambda_P| \quad (9)$$

for the fixed point to be a *stable node*⁶². Even though diagonalizing the *stability matrix* is a standard procedure in nonlinear dynamics, it is often computationally expensive⁶³, rendering it an impractical approach for the segregation. This necessitates the decoupling of the parameter space on the temporal hierarchy of the convergence timescale, which is computationally less expensive and fairly accurate (if not exact) with the following distinctive features^{44,46,47,64}-

- Principal Parameter Subset (*PPS*) $\{\theta_P\}$: Usually larger in magnitude, takes much more number of iterations to converge and a smaller subset.
- Auxiliary Parameter Subset (*APS*) $\{\theta_A\}$: Smaller in magnitude, converges much faster and a larger subset.

such that

$$N_P \ll N_A \quad (10)$$

whereas for the magnitude-based decoupling to hold, we require

$$|\theta_P| \gg |\theta_A| \quad (11)$$

Here we define the *principal parameter fraction* f_{pps} such that

$$f_{pps} = \frac{N_P}{N_{par}} \quad (12)$$

where, N_{par} is the total number of parameters. With the notion that such implicit partitioning of the parameter space exists^{44,46,47}, we may recast the disentangled unitary into two sub-parts \hat{U}_A and \hat{U}_P such that it forms a composite *principal-auxiliary bipartite* unitary (\hat{U}_{pab}) operator

$$\begin{aligned} \hat{U}_{pab} &= \hat{U}_P \cdot \hat{U}_A \\ &= \prod_{K=1}^{N_P} e^{\theta_{PK} \hat{\kappa}_{PK}} \prod_{\beta=1}^{N_A} e^{\theta_{A\beta} \hat{\kappa}_{A\beta}} \\ &= \left[\left(e^{\theta_{P_1}^D \hat{\kappa}_{P_1}^D} \dots e^{\theta_{P_I}^D \hat{\kappa}_{P_I}^D} \cdot e^{\theta_{P_J}^D \hat{\kappa}_{P_J}^D} \dots \right) \cdot \left(e^{\theta_{P_1}^S \hat{\kappa}_{P_1}^S} \dots e^{\theta_{P_K}^S \hat{\kappa}_{P_K}^S} \cdot e^{\theta_{P_L}^S \hat{\kappa}_{P_L}^S} \dots \right) \right] \left[\left(e^{\theta_{A_1}^D \hat{\kappa}_{A_1}^D} \dots e^{\theta_{A_\alpha}^D \hat{\kappa}_{A_\alpha}^D} \cdot e^{\theta_{A_\beta}^D \hat{\kappa}_{A_\beta}^D} \dots \right) \cdot \left(e^{\theta_{A_1}^S \hat{\kappa}_{A_1}^S} \dots e^{\theta_{A_\gamma}^S \hat{\kappa}_{A_\gamma}^S} \cdot e^{\theta_{A_\delta}^S \hat{\kappa}_{A_\delta}^S} \dots \right) \right] \end{aligned} \quad (13)$$

where, $\theta_*^{(S/D)}$ indicates parameters corresponding to singles or doubles excitations and P (A) are the *principal* (*auxiliary*) subscripts respectively. In the above expansion, both *principal* and *auxiliary* subsystem unitary operators are ordered according to their excitation rank (singles or doubles). Within each rank, the individual operators are arranged in regard to the relative absolute magnitude of the corresponding parameters such that in Eq. (13) we have $\theta_{P_I}^D > \theta_{P_J}^D$, $\theta_{P_K}^S > \theta_{P_L}^S$ and so on. The benefit of such an ordering will eventually be pronounced in the numerical analysis and comparative studies. Such parameter space decoupling leads to the discrete-time *equations of motion* of these two subsets as follows:

$$\Delta\theta_{A_\alpha} = \Lambda_{A_\alpha}\theta_{A_\alpha} + M_{A_\alpha}(\{\theta_P, \theta_A\}); \forall \alpha = 1, 2, \dots, N_A \quad (14)$$

and

$$\Delta\theta_{P_I} = \Lambda_{P_I}\theta_{P_I} + M_{P_I}(\{\theta_P, \theta_A\}); \forall I = 1, 2, \dots, N_P \quad (15)$$

Here, $\Lambda_\xi = \frac{1}{D_\xi} \langle \Phi_\xi | [\hat{H}, \hat{\kappa}_\xi] | \Phi_0 \rangle$ are the diagonal terms and $M_\xi(\{\theta_P, \theta_A\})$ contain all the off-diagonal and non-linearly coupled terms, where, depending on the context $\xi \in PPS$ or APS (see Appendix A for explicit expressions). Due to the nature of convergence, the time variation of the *auxiliary* parameters can be neglected (i.e. $\Delta\theta_{A_\alpha} = 0$ in Eq. (14)) via *adiabatic approximation*^{44,46,52,65} in the characteristic timescale of convergence of the *principal* parameters. Starting from Eq. (14) we can employ *adiabatic approximation* and relative magnitude condition (Eq. (11)) to immediately express the larger dimensional *auxiliary* parameters as a function of *principal* parameters only, which is succinctly captured in

$$\theta_{A_\alpha} = -\frac{M(\{\theta_P\})}{\Lambda_{A_\alpha}} = \frac{\langle \Phi_{A_\alpha} | \hat{U}_P^\dagger \hat{H} \hat{U}_P | \Phi_0 \rangle}{D_{A_\alpha}} \quad (16)$$

where,

$$\hat{U}_P(\{\theta_P\}) = \prod_I^{N_P} e^{\theta_{P_I} \hat{\kappa}_{P_I}} \quad (17)$$

is a *principal subsystem unitary* operator. The foundation of projecting the iterative trajectory into a lower-dimensional subspace hinges on the interrelationship depicted in Equation (16). The solution for *auxiliary* parameters (Eq. (16)) obtained from utilizing the *adiabatic approximation* provides a leading order approximation to the most general solution. The detailed derivation is shown in Appendix (A).

Having established the fact that the *auxiliary* amplitudes can be written solely as the function of the *principal* parameters upon the *adiabatic approximation*, one is essentially left with two choices. The most common practice in this scenario would be to invoke a *feedback coupling* where the updated auxiliary parameters (at each optimization step) contribute to the equations of the principal residues (or equivalently, principal parameters) via a

circular causality loop^{43,44,46,47}. While this method enables the estimation of *auxiliary* parameters using substantially shallower circuits, it requires the realization of a deep quantum circuit involving both *principal* and *auxiliary* parameters for *principal* residue constructions viz. $r_{P_I} = \langle \Phi_{P_I} | \hat{U}_{pab}^\dagger \hat{H} \hat{U}_{pab} | \Phi_0 \rangle$. An alternative approach in this direction would be to introduce a *no-feedback-controlled* equation for the principal amplitudes, which assumes that the optimization space spanned by the principal parameters is entirely decoupled from the rest. One, however, still needs to develop appropriate energy functional to account for the *auxiliary* parameters which are recessive to the optimization trajectory but have a significant contribution to the correlation energy. In the following section, we will invoke the *no-feedback-controlled* principal subspace evolution and would subsequently develop the theoretical framework that maps the evolved principal parameters towards a single-step updatation of the *auxiliary* parameters for quantitative accuracy.

B. No-feedback-controlled Evolution: Towards a shallow depth quantum algorithm

The above discussion describes how the usual synergistic *feedback-coupling* entails all the parameters for the principal residual, resulting in deeper circuit constructions. To circumvent this issue, we make a rather non-conservative assumption of *no-feedback-controlled evolution* of the principal parameters where the auxiliary parameters are assumed to have *no impact* on the optimization trajectory of the former. The validity for this assumption rests on two key attributes inherent to this class of nonlinear systems. Firstly, the fixed point θ^* of the iterative trajectory is a *stable node* and an *attracting fixed point*⁶². In other words, any initial point starting within the *basin of attraction*⁶² approach the fixed point i.e. $\theta_l \rightarrow \theta^*$ as $l \rightarrow \infty$. Secondly, the auxiliary parameters converge almost immediately and linger around the phase space trajectory⁶⁵ of the principal amplitudes till the residual condition is satisfied. These two properties justify considering the fixed point in the principal parameter phase space as approximately equivalent to the fixed point of the entire parameter space. As our interest solely lies in the fixed point properties of the iterative dynamics, the *no-feedback-controlled* approximation would emulate the overall dynamics quite accurately with auxiliary parameters mapped only at the convergence. These characteristics collectively ensure that a judiciously chosen principal subspace eventually lands on the *fixed point* in its phase space irrespective of the *feedback mechanism*. It should be emphasized that without the *feedback coupling*, proper choice of the *principal* subspace is extremely important otherwise, it might lead to imprecise evolution and inaccurate *auxiliary* parameter mapping.

Assuming that one identifies the appropriate set of *principal* parameters, one may construct the residue vector corresponding to the subspace spanned solely by

the *principal* parameters, disregarding the contributions from the *auxiliary* parameters:

$$r_{P_I} \approx \langle \Phi_{P_I} | \hat{U}_P^\dagger \hat{H} \hat{U}_P | \Phi_0 \rangle \quad (18)$$

At this point, it is worth noting the difference between the *no-feedback-controlled* generation of the principal residue vectors and the *feedback-controlled* generation: in the case of the latter, one needs to construct the effective Hamiltonian where both principal and auxiliary parameters contribute, resulting in a proliferation of the circuit depth. This is prudently bypassed in the no-feedback-controlled generation as exemplified in Eq. (18).

With the optimized *principal* parameters, one may determine the *auxiliary* parameters through Eq. (16) post optimization. One begging question at this juncture is to develop an appropriate energy expression that can in principle account for the correlation energy accurately at the cost of a shallow *fixed-depth-circuit*. With the assumption that the *principal* and *auxiliary* subspaces remain entirely uncoupled, the contributions of the *auxiliary* parameters to energy are to be treated as additional extraneous corrections. Leveraging the principal-auxiliary bipartite structure of the unitary, under magnitude-based parameter decoupling, one may partially transform the bare Hamiltonian to a transformed Hamiltonian $\bar{H}_P = U_P^\dagger \hat{H} U_P$ by employing the Baker-Campbell-Hausdorff expansion and restricting the contributions of the *auxiliary* parameters at the second power. The energy expression then takes the form -

$$\begin{aligned} E = & \langle \Phi_0 | \left(\prod_{PPS}^{N_P} e^{\theta_P \hat{\kappa}_P} \prod_{APS}^{N_A} e^{\theta_A(\{\theta_p\}) \hat{\kappa}_A} \right)^\dagger \hat{H} \\ & \left(\prod_{PPS}^{N_P} e^{\theta_P \hat{\kappa}_P} \prod_{APS}^{N_A} e^{\theta_A(\{\theta_p\}) \hat{\kappa}_A} \right) | \Phi_0 \rangle \\ = & \langle \Phi_0 | \bar{H}_P | \Phi_0 \rangle + \sum_{A_\alpha \in APS} \theta_{A_\alpha} \underbrace{\langle \Phi_0 | [\bar{H}_P, \hat{\kappa}_{A_\alpha}] | \Phi_0 \rangle}_{\text{Term 1}} \\ & + \frac{1}{2} \sum_{A_\alpha, A_\beta} \theta_{A_\alpha} \theta_{A_\beta} \underbrace{\langle \Phi_0 | [[\bar{H}_P, \hat{\kappa}_{A_\alpha}], \hat{\kappa}_{A_\beta}] | \Phi_0 \rangle}_{\text{Term 2}} \end{aligned} \quad (19)$$

Here, $\theta_A(\{\theta_P\})$ denote that the *auxiliary* parameters (θ_A) are not independent but rather are derived from the *principal* parameters (θ_p) using Eq. (16). After simplifying *Term 1* and *Term 2* in Eq. (19) (see Appendix C), the final energy may be written as:

$$E \approx \langle \Phi_0 | \hat{U}_P^\dagger \hat{H} \hat{U}_P | \Phi_0 \rangle + \sum_{\alpha=1}^{N_A} \theta_{A_\alpha}^2 D_{A_\alpha} \quad (20)$$

Eq. (20), combined with Eqs. (18) and (16) gives the entire protocol for performing *no-feedback-controlled adiabatically decoupled* PQE (*nfcAD-PQE*). With the formalism developed so far, the *nfcAD-PQE* can be outlined with the following sequential steps-

1. The initial estimate for the single and double excitation parameters are chosen based on their leading order values. This implies that the doubles are estimated based on their magnitudes at the first order while the singles are estimated from the second perturbative order³⁰. Under the magnitude-based decoupling at this step, the parameter space is partitioned into *PPS* and *APS* according to the ordering in Eq. (13). The parameter set is sorted based on their absolute magnitude while keeping track of their corresponding excitation indices. We set the value of f_{pps} such that *PPS* contains the largest $N_P = f_{pps} N_{par}$ parameters. The remaining $N_A = (N_{par} - N_P)$ number of parameters constitute *APS*.

2. Only the principal parameters are updated with the residue defined in Eq. (18) till convergence

$$\theta_{P_I}^{(k+1)} = \theta_{P_I}^{(k)} + \frac{r_{P_I}^{(k)}}{D_{P_I}}. \quad (21)$$

3. As the residual condition $r_{P_I} \rightarrow 0$ is satisfied, the iteration over the principal subspace is terminated. At this fixed point in the principal parameter phase space, the auxiliary parameters are mapped via one-step *post-optimization mapping* using Eq. (16). Finally, the energy is determined via the approximated equation Eq. (20).

In contrast to measurement-based methods like ADAPT-VQE or SPQE, *nfcAD-PQE* does not discard operators from the pool but transfers them to an auxiliary subspace with a degree of approximation without needing additional selection measurements or quantum resources. Additionally, instead of treating *nfcAD-PQE* and SPQE or ADAPT-VQE as two competing theories, the former can be integrated with dynamic ansatz algorithms^{16,31} for even greater resource efficiency. In the following subsection, we delve into a detailed discussion about the reduced resource requirements of *nfcAD-PQE* and its quantifiable impact in scenarios with noise.

C. Advantages of *nfcAD-PQE*

Reduction in number of measurements

The primary advantage inherent in the application of *nfcAD-PQE* lies in its exclusive optimization of the *principal* subset. This subspace optimization strategy results in a drastic reduction in the number of residue component evaluations, which has explicit effects on the number of measurements. Quantitatively, the number of measurements (m_{res}) needed to compute the residual vector involving N_{par} parameters with precision ϵ has an upper bound^{31,66}

$$m_{res} \leq 3N_{par} \frac{(\sum_l |h_l|)^2}{\epsilon^2} \quad (22)$$

where h_l is the coefficient of the l -th Pauli string in the Jordan-Wigner-mapped Hamiltonian. Consequently, the ratio between the number of measurements utilized by *nfcAD-PQE* to that of conventional *PQE* (per residue vector evaluation) approximately becomes

$$\frac{m_{res}^{nfcAD-PQE}}{m_{res}^{PQE}} = f_{pps} < 1 \quad (23)$$

which translates into significant reduction in measurement costs when implemented throughout the entire iterative process until convergence is achieved. Along this line, one must also note that *nfcAD-PQE*, being static structured, does not require any *pre-circuit measurements* towards the operator selection, and this turns out to be of immense advantage over measurement-based ansatz construction in noisy quantum devices.

Reduction in gate depth

Minimizing the number of CNOT gates stands as a paramount objective for any NISQ-friendly algorithm. In the case of a serial implementation of dUCCSD ansatz construction with Jordan-Wigner mapping, the number of gates (mainly CNOT) scales as⁶⁷ $\sim N^5$, where N is the number of qubits. However, with *nfcAD-PQE*, where circuits are parameterized solely by the *principal parameters*, the gate requirement diminishes to around $\sim f_{pps}N^5$. In practical terms, this translates to significant reductions in CNOT gates since $f_{pps} < 1$. CNOT gates are extremely susceptible to noise in hardware realizations. Therefore, reducing the number of CNOT gates ultimately enhances performance in realistic scenarios, promising more robust outcomes.

Reduced impact of noise

The focus of the algorithm on enhanced applicability under noise motivates a discussion on the mathematical relationship between noise and circuit depth. Noise can be modeled by discrete probabilistic events called *faults* that can occur at a variety of locations in a quantum circuit^{68,69}. Considering Pauli noise with probability p_l at circuit location l , the probability that no fault occurs (or the *fault-free probability* is⁷⁰) $P_0 = \prod_l (1 - p_l)$. For a measure of the amount of noise, we can define the average number of circuit faults per run or the *circuit fault rate* $r = \sum_l p_l$. For a circuit with location-independent Pauli noise probability p the circuit fault rate becomes $\lambda = Lp$, where L is the total number of *fault locations* and the corresponding *fault free probability* is $P_0 = e^{-Lp}$. As we have already discussed in section III A, the number of

CNOT gates is a rough estimate of the number of *fault locations* in a circuit which scales as $\sim N^5$ for *PQE* and $\sim f_{pps}N^5$ for *nfcAD-PQE*. The corresponding *fault free probabilities* are

$$\begin{aligned} P_0^{(PQE)} &\sim e^{-N^5} \\ P_0^{(nfcAD-PQE)} &\sim e^{-f_{pps}N^5} \end{aligned} \quad (24)$$

respectively. Due to the presence of the fraction f_{pps} , the fault-free probability for *nfcAD-PQE* ($P_0^{(nfcAD-PQE)}$) clearly decays much slower than that of *PQE* ($P_0^{(PQE)}$) indicating less accumulation of noise in *nfcAD-PQE* framework for NISQ platforms.

Improved efficacy towards Error Mitigation

To obtain meaningful accuracy in computations performed in noisy quantum hardware, one must apply additional layers of error mitigation methods. Zero Noise Extrapolation (ZNE)^{71,72} stands out as one of the most widely used methods to mitigate gate-based errors. It retrieves the expectation value of an operator by extrapolating to zero noise limit from the data obtained through constructing the quantum circuit at various effective degrees of processor noise. However, the efficacy of ZNE and the quality of error mitigation deteriorate with the increasing depth of the circuit. For ZNE with n -th order Richardson extrapolation method, the upper bound of the error for the zero noise estimate is $\sim \mathcal{O}((NTr)^{n+1})$ ^{73,74}, where N is the number of qubits and T is the total evolution time. Therefore, for a pronounced efficacy of ZNE, a smaller NTr is required. *nfcAD-PQE* furnishes a low value of r as compared to conventional *PQE*. Thus, for *nfcAD-PQE*, the upper bound for the error in the zero noise estimate becomes $\mathcal{O}(f_{pps}^{n+1}(NTr)^{n+1})$. Due to the conditions $f_{pps} < 1$ and $n > 1$, the extrapolation error bound for ZNE is analytically shown to be reduced, which translates to a more pronounced efficiency of ZNE in *nfcAD-PQE*. Moreover, the *sampling cost* of an error mitigation protocol is also tremendously minimized as it grows exponentially with circuit depth⁷⁵.

Having analytically established the multi-fold advantages of *nfcAD-PQE* implementation at a reduced quantum complexity, we will analyze its accuracy in the next section. Towards this, we shall discuss the results of quantum simulations under synthetic device noise as well as in ideal quantum simulators, and this will demonstrate the superiority of the algorithm over allied methods to decipher its short and long-term benefits.

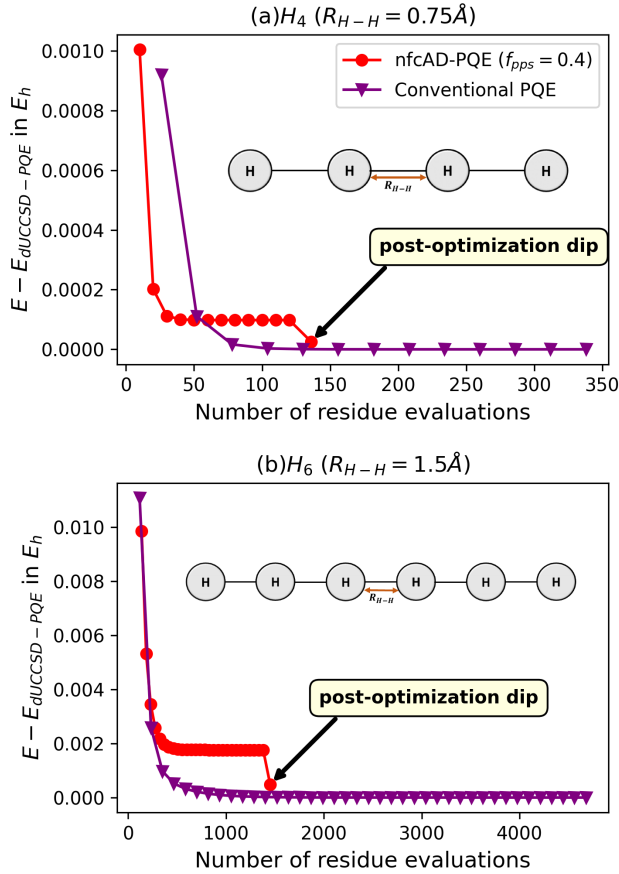


FIG. 1. Convergence profile of *nfcAD*-PQE against the conventional dUCCSD-PQE for (a) H_4 ($R_{H-H} = 0.75\text{\AA}$) and (b) H_6 ($R_{H-H} = 1.5\text{\AA}$) in STO-3G basis. The post-optimization dip is the signature of single-step mapping to incorporate auxiliary amplitudes.

III. RESULTS AND NUMERICAL ANALYSIS

A. *nfcAD*-PQE Under Noiseless Environment: Numerical Demonstrations of its Robustness for the Fault-tolerant Era

In this section, we demonstrate the performance of *nfcAD*-PQE under the ideal noiseless scenario that sets the ultimate limit of the algorithm for the fault-tolerant era. For this, we will be comparing the accuracy of *nfcAD*-PQE with respect to the conventional PQE which has been established as an accurate resource-efficient alternative to VQE. We perform this study for a number of molecules with varied electronic complexities. All the numerical simulations are performed using in-house codes interfaced with Qiskit⁷⁶. The molecular orbitals and requisite integrals are imported from PySCF⁷⁷. For all our applications, we have used STO-3G basis and the rank of the excitation operators is truncated at the singles and doubles (SD). Furthermore, a convergence threshold of 10^{-5} for the residue norm has been used uniformly and

no additional convergence accelerating technique (such as DIIS) is used.

To illustrate the convergence profile of *nfcAD*-PQE, in Fig. 1, we present the optimization landscape of (a) linear H_4 and (b) linear H_6 with $H - H$ distance set to be 0.75\AA and 1.5\AA respectively with f_{pps} taken to be 0.4. Fig. 1 also contains the energy trajectory for conventional PQE. We reiterate that *nfcAD*-PQE assumes the existence of a fixed point within the principal parameter subspace that closely represents the global fixed point of the entire set of parameters. The optimization is thus restricted within a disjoint principal parameter subspace, manifesting in a drastic reduction in the number of total residue component evaluations of the residual vector r_μ as predicted quantitatively in section II C. Furthermore, *nfcAD*-PQE crucially depends upon the post-optimization mapping of the *auxiliary* parameters from the principal ones (Eq. 16). These two sets of parameters collectively contribute to the energy function once the fixed point within the principal subspace is reached. This manifests in a distinctive post-optimization dip in the energy landscape, ensuring its characteristic accuracy compared to conventional dUCCSD-PQE. Moreover, it achieves this while requiring an order of magnitude fewer residue evaluations, resulting in fewer measurements as analytically established in II C.

To assess the accuracy, in Fig. 2 we have studied the potential energy profiles of three challenging molecular systems (a) stretching of linear H_4 , (b) symmetric stretching of CH_2 and (c) stretching of linear H_6 . In order to numerically validate the resource efficiency of *nfcAD*-PQE, we have compared its accuracy with selected PQE (SPQE)³¹ – a measurement-based ansatz compactification protocol within the PQE framework. To ensure a fair comparison, we constrained the SPQE operator pool to only include single and double (SD) excitations, with an importance selection threshold of $\Omega = 0.01$, and a time-length of $\Delta t = 0.9$ for the unitary evolution. For a detailed discussion on SPQE, we refer to the work by Evangelista and co-workers^{31,38}.

The first row in Fig. 2 represents the energy values of *nfcAD*-PQE or SPQE with respect to dUCCSD-PQE for different inter-atomic distances. The second and third row shows the number of CNOT gates and the number of parameters respectively used in *nfcAD*-PQE, SPQE, and conventional dUCCSD-PQE. For near-equilibrium geometries of linear H_4 , SPQE ($\Omega = 0.01$) performs better than *nfcAD*-PQE ($f_{pps} = 0.4$ and 0.5). While at stretched geometries, where strong correlation effects prevail, *nfcAD*-PQE is more accurate as the choice of principal parameters along with the *post-optimization mapping* recovers better electronic correlation even with less number of parameters and CNOT gates. In the case of CH_2 , *nfcAD*-PQE with $f_{pps} = 0.3$ is more accurate than SPQE throughout the surface. However, the former has slightly higher parameters and gate counts. Similar trend is observed in H_6 where *nfcAD*-PQE ($f_{pps} = 0.5$) contains almost the same number of parameters as that of

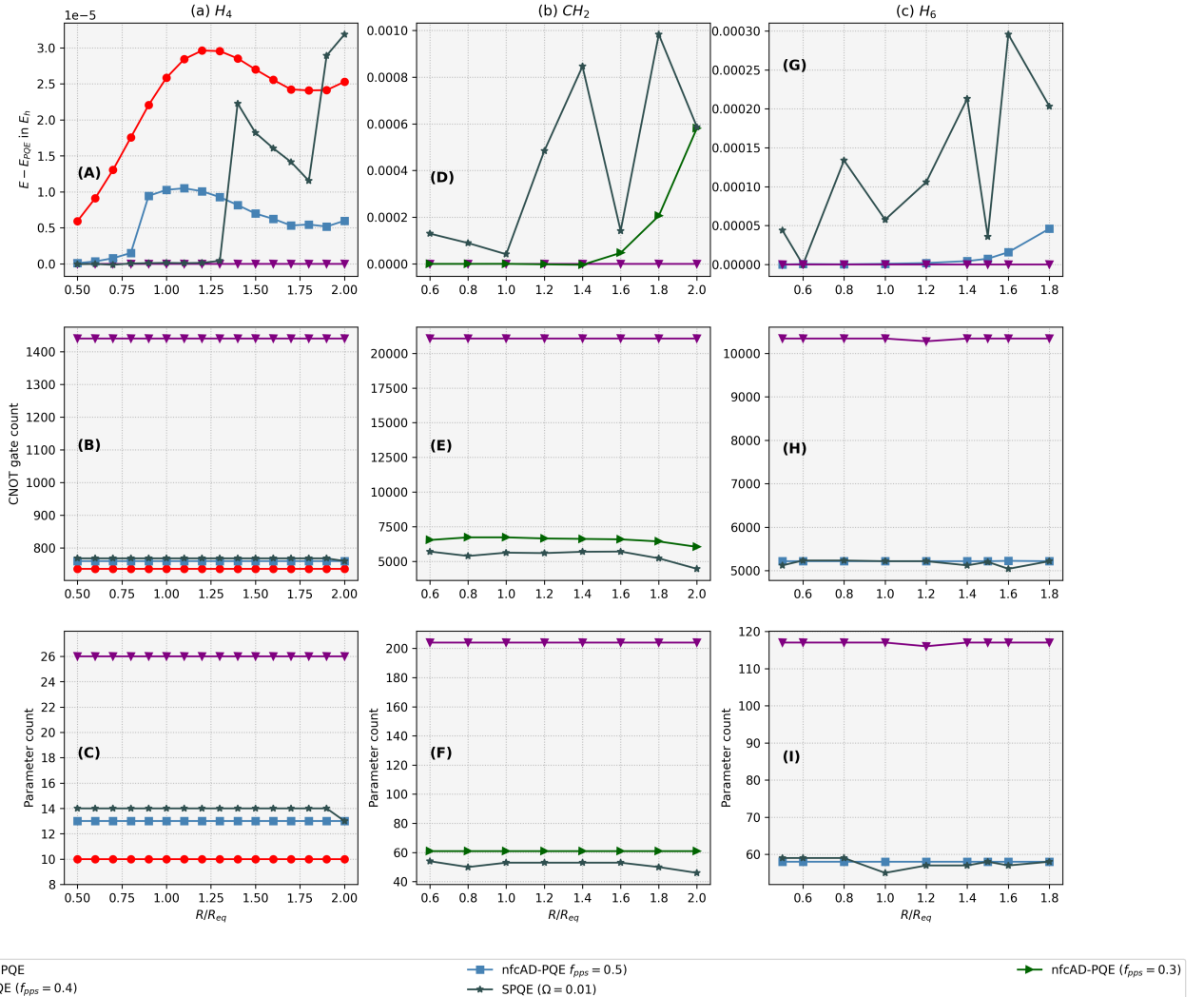


FIG. 2. Potential energy surface for (a) H_4 ($R_{(eq)H-H} = 0.75\text{\AA}$), (b) CH_2 ($\angle C - H - C = 102.4^\circ$, $R_{(eq)C-H} = 1.1096\text{\AA}$) and (c) H_6 ($R_{(eq)H-H} = 0.75\text{\AA}$) in STO-3G basis. The SPQE algorithm is implemented with threshold $\Omega = 0.01$ and time evolution parameter $\Delta t = 0.9s$. To keep things on an equal footing, the operator pool for SPQE is restricted to singles and doubles. The principal fraction used for nfcAD-PQE ranges from $f_{pps} = 0.3$ to 0.5 . The first row (A,D,G) represents the energy of each individual method (nfcAD-PQE and SPQE) with respect to dUCCSD-PQE converged energy (E_{PQE}) for different inter-atomic separations. The corresponding number of CNOT gates (B,E,H) and parameter counts (C,F,I) are also shown for each respective point along the potential energy profile.

SPQE but is better in accuracy. Although nfcAD-PQE comes with a shallow circuit with static structure and operator ordering, it is capable of capturing correlation uniformly over the potential energy profile, as corroborated by very small non-parallelity error (NPE). Here, we emphasize the fact that we aim to attain the characteristic accuracy of the parent ansatz (dUCCSD-PQE in this case) with lower quantum resources, and thus, we refrain from comparing against FCI. However, our approach is entirely general and the adaptability of the al-

gorithm does not depend on the parameterization of the ansatz.

In summary, all of our numerical simulations in Fig. 2 demonstrate that within the range of $f_{pps} = 0.3 - 0.5$, nfcAD-PQE shows an accuracy of the range $10^{-6}\text{--}10^{-4}E_h$ to dUCCSD-PQE, albeit at an order-of-magnitude reduction in the number of residue evaluations, number of parameters and, consequently, the CNOT gate count. In this regard, it is on par with SPQE in terms of accuracy and quantum resource utilization,

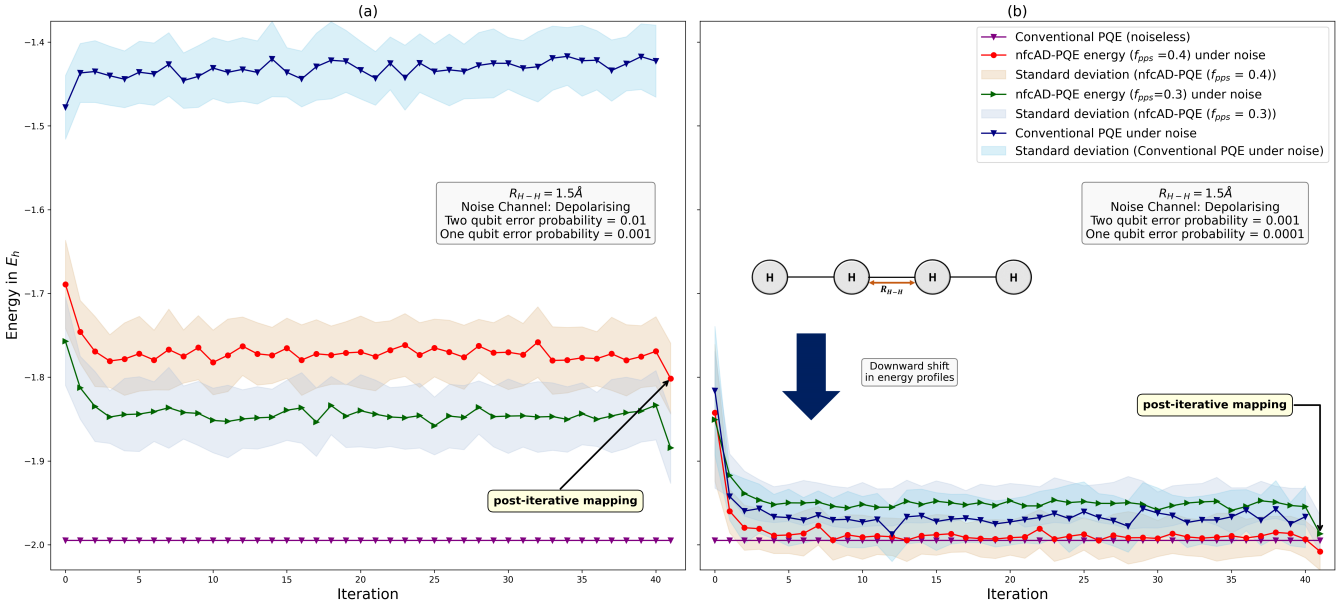


FIG. 3. Energy optimization landscape for *nfc*AD-PQE and conventional PQE using dUCCSD ansatz under depolarising noise channels for linear H_4 ($R_{H-H} = 1.5\text{\AA}$) in STO-3G basis. The study was performed with two different strengths of depolarising error parameters, as mentioned in the inset of the subplots. For every requisite expectation value, the number of shots was set to 5000. (a) With current hardware noise, *nfc* AD-PQE shows distinct signature of convergence with significantly lower energy profiles than dUCCSD-PQE and the characteristic *post-optimization dip*. (b) With one order synthetic reduction of the hardware noise, the energy profiles for *nfc*AD-PQE show qualitatively similar behavior to that of an ideal noiseless scenario as the electronic correlation effects start to predominate.

however, with the added advantage of zero pre-circuit measurement— a significant advantage for the utility of the method in noisy devices. Furthermore, the accuracy of *nfc*AD-PQE is systematically improvable with f_{pps} , and this provides us with enough additional flexibility to fine-tune our approach depending on the degree of accuracy warranted by the chemical system. In the next section, we will numerically demonstrate the robustness of *nfc*AD-PQE in the noisy environment.

B. *nfc*AD-PQE in NISQ Platforms: Numerical Simulations with Depolarizing Noise Channel

The accuracy of *nfc*AD-PQE, observed under noise-free conditions (that marks the fault-tolerant era), serves to validate the robustness of the underlying assumptions employed towards the genesis of its working equations. However, the real advantage of this approach becomes evident when the proposed methodology is employed in NISQ environment. At this juncture, one must note that the selection and the partitioning of the operators in the unitary ansatz are performed based on their magnitudes at the MP2 level. Thus, unlike methods that rely on pre-circuit measurements to come up with an optimal ansatz, our ansatz is static, and it remains structurally unaffected in NISQ environment.

Fig. 3 depicts the optimization landscape of *nfc*AD-PQE for H_4 ($r_{H-H} = 1.5\text{\AA}$) under depolarizing noise

(which is one of the dominant sources of error in NISQ hardware). For all the computations depicted in Fig 3, ZNE with random gate folding and Richardson extrapolation (with scale factors [1,2,3]) was employed throughout to compute all expectation values as an error mitigation protocol. It was implemented using routines from Mitiq⁷⁸. While performing computations under noise (for both PQE and *nfc*AD-PQE), we have further exploited qubit excitation-based (QEB) CNOT efficient quantum circuits^{37,38} for realizing the dUCCSD ansatz. This is done to further reduce the CNOT gate counts for better implementation of ZNE. Owing to disruptive noisy fluctuations, the iterative method fails to converge to a stable fixed point. In such a scenario, in this simulation, the iteration was terminated at iterative counter value 40. At the termination point of each iteration, we take the average of principal parameters for the preceding 10 iterations and with that averaged set of *principal* parameters the *auxiliary* parameters are mapped. Given the stochastic nature of energy values at each iteration, we conducted 50 independent runs, computing the average with the corresponding standard deviation as shown in Fig. 3. From Fig. 3(a), it can be discerned how *nfc*AD-PQE produces better performance under noise than conventional dUCCSD-PQE with significantly lower energy profile. With present-day hardware noise, conventional PQE shows no convergence signature, while for *nfc*AD-PQE, a distinct convergence signature is followed by a discernible *post-optimization mapping* dip. The improved accuracy

for *nfcAD-PQE* may be attributed to a combined effect of less accumulation of noise due to the reduction in the number of fault locations and lower ZNE extrapolation error bounds, as discussed in section II C. Surprisingly, at the current hardware noise level, Fig. 3(a) shows *nfcAD-PQE* with lower f_{pps} is more accurate, contrary to the ideal environment scenario (Fig. 2). A plausible explanation for this is that, at the current level of hardware noise, a shallower quantum circuit, attributed to fewer *fault locations*, yields superior results even though such an ansatz is not adequately expressive to capture accurate many-body correlation and thus, such superior performance with a sub-optimally parameterized ansatz is an artifact of a high degree of hardware noise. With an improvement in the quantum hardware, such a sub-optimally parameterized ansatz would be less accurate, and the energy computation would be more dominated by electronic correlation effects, ultimately leading to the noiseless results discussed in section III A. To numerically demonstrate such a transition, in Fig. 3(b) we have simulated the algorithms with one order-of-magnitude less depolarizing error parameters. Expectedly, the results reveal a downward shift in the overall energy profiles, commencing a trend that qualitatively shows the behavior illustrated in Fig. 2. At this lower noise intensity the *nfcAD-PQE* with $f_{pps} = 0.4$, despite containing deeper circuits is more accurate than its other counterparts under consideration. Such an observation suggests that, in this case, the choice of the principal parameter subspace is optimal to maintain a better trade-off between handling errors due to noise while concurrently capturing the requisite electronic correlation energy. The one with $f_{pps} = 0.3$ is still showing better average accuracy (after the *post-optimization mapping*) compared to conventional PQE. However, it starts to exhibit a comparatively upward shift, indicative of its sub-optimal *principal subspace* parameterization when it comes to the energy estimation under ideal circumstances. Thus, it is imperative that the principal subspace is optimally parameterized to strike the right balance, and our numerical investigation shows that $f_{PPS} = 0.4$ is the optimal principal fraction in this regard.

To summarize, our numerical investigations establish the imperative that *nfcAD-PQE* strikes a balance between two extremely important aspects. It has better capability to efficiently handle noise-induced errors for more effective integration into the currently available NISQ devices while being requisitely precise enough to reproduce characteristic accuracy in ideal noiseless conditions. With the improvement in quantum hardware in the near future, this balance would play a pivotal role in extracting useful information and harnessing the advantages of quantum speed-up for practical utility.

IV. CONCLUSION AND FUTURE OUTLOOK

In this work, we have devised the *nfcAD-PQE* formalism that has its roots in principles of *synergetics* and *non-linear dynamics* for a resource-efficient projective quantum algorithm. The method considers the projective parameter optimization problem as discrete-time iterative dynamics and fundamentally relies upon the *adiabatic decoupling* of the dominant *principal* and the submissive *auxiliary* modes based on their hierarchical timescale of convergence. The application of *adiabatic elimination* enables the isolation of the *principal* parameter subspace from the remaining system components. This allows us to study the unitary evolution of the whole system in a significantly reduced dimensional subspace. We design an accurate theoretic technique that maps the *principal* amplitudes to the *auxiliary* ones with *no-feedback-control* assumption that naturally guides us to construct the energy functional with a shallow depth fixed structured circuit. We have analytically established that *nfcAD-PQE* requires fewer measurements, a reduced number of CNOT gates, and is less affected by hardware noise, which results in better error mitigability when integrated with ZNE when compared to its conventional counterpart. Under an ideal fault-tolerant environment, the proposed methodology is capable of capturing balanced correlation effects for molecules with varied electronic complexity while concurrently maintaining requisite accuracy in NISQ environment, albeit at a significantly lower quantum complexity and without the requirements of any pre-circuit quantum measurements to come up with an optimal ansatz. We hope that with the development of better quantum computing infrastructures along with efficient and more accurate quantum error mitigation protocols, *nfcAD-PQE* will give rise to even more accurate results towards the exploration of novel chemical space.

V. ACKNOWLEDGMENTS

RM acknowledges the financial support from Industrial Research and Consultancy Centre, IIT Bombay, and Science and Engineering Research Board, Government of India. CP acknowledges UGC (University Grants Commission and SH thanks CSIR (Council of Scientific and Industrial Research) for their respective fellowships.

AUTHOR DECLARATIONS

Conflict of Interest:

The authors have no conflict of interest to disclose.

DATA AVAILABILITY

The data is available upon reasonable request to the corresponding author.

Appendix A: Generalized solution of the auxiliary parameters and validity of the adiabatic approximation

In this appendix, we discuss the validity of the adiabatic approximation from the most general solution for the auxiliary parameters. The discrete-time dynamical equations for the parameters have the general form

$$\Delta\theta_\xi = \Lambda_\xi\theta_\xi + M_\xi(\{\theta_P, \theta_A\}) \quad (\text{A1})$$

Here, diagonal and off-diagonal terms can be expressed by:

$$\Lambda_\xi = \frac{1}{D_\xi} \langle \Phi_\xi | [\hat{H}, \hat{\kappa}_\xi] | \Phi_0 \rangle \quad (\text{A2})$$

$$\begin{aligned} M_\xi(\{\theta_P, \theta_A\}) &= \frac{1}{D_\xi} \langle \Phi_\xi | \hat{H} + \sum_{\nu \neq \xi} \theta_\nu [\hat{H}, \hat{\kappa}_\nu] \\ &+ \sum_{\nu} \sum_{\mu > \nu} \theta_\nu \theta_\mu [[\hat{H}, \hat{\kappa}_\nu], \hat{\kappa}_\mu] + \dots | \Phi_0 \rangle \end{aligned} \quad (\text{A3})$$

where, depending on the context $\xi \in PPS$ or APS . Note that in both the equations above, we have not yet imposed any restrictions on the labels μ, ν . The most general solution to the *auxiliary* parameter equation Eq. (14) can be immediately written as⁷⁹

$$\theta_{A_\alpha} = \sum_{m=-\infty}^l (1 + \Lambda_{A_\alpha})^{l-m} M_{A_\alpha} \quad (\text{A4})$$

By definition Λ_{A_α} (Eq. (A2)) is in general negative (see Appendix B), ensuring the convergent series expansion of the *auxiliary* modes. Starting from Eq. (A4), we can employ *summation by parts* to further simplify⁷⁹-

$$\begin{aligned} \theta_{A_\alpha} &= M_{A_\alpha} \sum_{m=-\infty}^l (1 + \Lambda_{A_\alpha})^{l-m} \\ &- \sum_{m=-\infty}^l (1 + \Lambda_{A_\alpha})^{l+1-m} \sum_{m'=-\infty}^{m-1} (1 + \Lambda_{A_\alpha})^{m-1-m'} \Delta M_{A_\alpha} \end{aligned} \quad (\text{A5})$$

Carrying out the summations in Eq. (A5) leads to the final solution for the auxiliary modes

$$\theta_{A_\alpha} = -\frac{M(\{\theta_P, \theta_A\})}{\Lambda_{A_\alpha}} - \frac{\Delta M(\{\theta_P, \theta_A\})}{\Lambda_{A_\alpha}^2} \quad (\text{A6})$$

However, due to the nature of convergence, the time variation of the auxiliary modes can be neglected (i.e. $\Delta\theta_{A_\alpha} = 0$ in Eq. (14)) via *adiabatic approximation*^{44,46,52,65} in the characteristic timescale of convergence of the *principal* parameters. Starting from Eq. (14) we can employ *adiabatic approximation* to immediately get the *auxiliary* mode solution

$$\theta_{A_\alpha} = -\frac{M(\{\theta_P, \theta_A\})}{\Lambda_{A_\alpha}} \quad (\text{A7})$$

Further, the relative magnitude condition (Eq. (11)) can be invoked to express the *auxiliary* parameters as a function of *principal* parameters only

$$\theta_{A_\alpha} = -\frac{M(\{\theta_P, \theta_A\})}{\Lambda_{A_\alpha}} \xrightarrow{|\theta_A| \ll |\theta_P|} -\frac{M_{A_\alpha}(\{\theta_P\})}{\Lambda_{A_\alpha}} \quad (\text{A8})$$

From Eq. (A3) one can write $M_{A_\alpha}(\{\theta_P\})$ explicitly as

$$\begin{aligned} M_{A_\alpha}(\{\theta_P\}) &\approx \frac{1}{D_{A_\alpha}} \langle \Phi_{A_\alpha} | \hat{H} + \sum_{P_I} \theta_{P_I} [\hat{H}, \hat{\kappa}_{P_I}] \\ &+ \sum_{P_I} \sum_{P_J > P_I} \theta_{P_I} \theta_{P_J} [[\hat{H}, \hat{\kappa}_{P_I}], \hat{\kappa}_{P_J}] + \dots | \Phi_0 \rangle \\ &= -\frac{\langle \Phi_{A_\alpha} | \hat{U}_P^\dagger(\{\theta_P\}) \hat{H} \hat{U}_P(\{\theta_P\}) | \Phi_0 \rangle}{\langle \Phi_{A_\alpha} | [\hat{H}, \hat{\kappa}_{A_\alpha}] | \Phi_0 \rangle} \end{aligned} \quad (\text{A9})$$

Using this Eq. (A8) can be compactly written as-

$$\begin{aligned} \theta_{A_\alpha} &= -\frac{\langle \Phi_{A_\alpha} | \hat{U}_P^\dagger(\{\theta_P\}) \hat{H} \hat{U}_P(\{\theta_P\}) | \Phi_0 \rangle}{\langle \Phi_{A_\alpha} | [\hat{H}, \hat{\kappa}_{A_\alpha}] | \Phi_0 \rangle} \\ &= \frac{\langle \Phi_{A_\alpha} | \hat{U}_P^\dagger(\{\theta_P\}) \hat{H} \hat{U}_P(\{\theta_P\}) | \Phi_0 \rangle}{D_{A_\alpha}} \end{aligned} \quad (\text{A10})$$

where, $\hat{U}_P(\{\theta_P\})$ is defined in Eq. (17) and $\langle \Phi_{A_\alpha} | [\hat{H}, \hat{\kappa}_{A_\alpha}] | \Phi_0 \rangle \approx -D_{A_\alpha}$ under leading order approximation (see Appendix (B) for the validity of the approximation). A direct comparison of Eq. (A10) with (A6) reveals that the *adiabatic approximation* (Eq. (A10)) constitutes the leading order term of the generalized solution, indicating its considerable accuracy⁴¹.

Appendix B: Approximation of the commutator terms and convergence criteria for series expansion of auxiliary mode solutions

In this section, we provide a mathematical rationale behind the convergence of the most general solution (Eq. (A4)) along with the validity of the particular compact structure of the denominator in Eq. (16). The commutator of the form $\langle \Phi_\mu | [\hat{H}, \hat{\kappa}_\nu] | \Phi_0 \rangle$ can be approximated by expanding the Hamiltonian into a zeroth order one-body Fock operator and first order two-body operator $\hat{H} = \hat{F}^{(0)} + \hat{V}^{(1)}$ and keeping the zeroth order term only

$$\begin{aligned} &\langle \Phi_\mu | [\hat{H}, \hat{\kappa}_\nu] | \Phi_0 \rangle \\ &\implies \langle \Phi_\mu | [\hat{F}^{(0)}, \hat{\kappa}_\nu] | \Phi_0 \rangle \approx -D_\mu \delta_{\mu\nu} \end{aligned} \quad (\text{B1})$$

The definition of the coefficient of the linear terms has the generic form-

$$\Lambda_\mu = \frac{1}{D_\mu} \langle \Phi_\mu | [\hat{H}, \hat{\kappa}_\mu] | \Phi_0 \rangle \quad (\text{B2})$$

From the results of Eq. (B1) we can see that Λ_μ is negative and $|\Lambda_\mu| \sim 1$ such that $|1 + \Lambda_\mu| << 1$ ensuring the convergence of the series in Eq. (A4).

Appendix C: Derivation of the low depth energy determining equation

Here, we analytically establish the energy expression (Eq. (20)) for a shallow-depth utilization. With the *principal-auxiliary bipartite* operator (Eq. (13)), the energy term can be expressed by

$$E_{AD-PQE}(\boldsymbol{\theta}) = \langle \Phi_0 | \hat{U}_{pab}^\dagger(\boldsymbol{\theta}) H \hat{U}_{pab}(\boldsymbol{\theta}) | \Phi_0 \rangle \quad (\text{C1})$$

Term 1 and Term 2 in Eq. (19) can be further expanded-

Term 1

$$\begin{aligned} & \langle \Phi_0 | [\bar{H}_P, \hat{\kappa}_{A_\alpha}] | \Phi_0 \rangle \\ &= \langle \Phi_0 | \bar{H}_P \hat{\kappa}_{A_\alpha} | \Phi_0 \rangle - \langle \Phi_0 | \hat{\kappa}_{A_\alpha} \bar{H}_P | \Phi_0 \rangle \\ &= \langle \Phi_0 | \bar{H}_P | \Phi_{A_\alpha} \rangle + \langle \Phi_{A_\alpha} | \bar{H}_P | \Phi_0 \rangle \\ &= 2 \langle \Phi_{A_\alpha} | \hat{U}_P^\dagger \hat{H} \hat{U}_P | \Phi_0 \rangle \\ &= 2\theta_{A_\alpha} D_{A_\alpha} \end{aligned} \quad (\text{C2})$$

where, at the last step we have used Eq. (16) to replace the operator expectation value with adiabatically obtained auxiliary parameters.

Term 2

Since term 2 is a nonlinear term, for its evaluation we first approximate the BCH expansion for \bar{H}_P up to zeroth order and then follow the second quantized operator algebra for the final compact form-

$$\begin{aligned} & \langle \Phi_0 | [\bar{H}_P, \hat{\kappa}_{A_\alpha}], \hat{\kappa}_{A_\beta} | \Phi_0 \rangle \\ & \approx \langle \Phi_0 | [\hat{H}, \hat{\kappa}_{A_\alpha}], \hat{\kappa}_{A_\beta} | \Phi_0 \rangle \\ &= \langle \Phi_0 | [\hat{H}, \hat{\kappa}_{A_\alpha}] \hat{\kappa}_{A_\beta} | \Phi_0 \rangle - \langle \Phi_0 | \hat{\kappa}_{A_\beta} [\hat{H}, \hat{\kappa}_{A_\alpha}] | \Phi_0 \rangle \quad (\text{C3}) \\ &= \langle \Phi_0 | [\hat{H}, \hat{\kappa}_{A_\alpha}] | \Phi_{A_\beta} \rangle + \langle \Phi_{A_\beta} | [\hat{H}, \hat{\kappa}_{A_\alpha}] | \Phi_0 \rangle \\ &= 2 \langle \Phi_{A_\beta} | [\hat{H}, \hat{\kappa}_{A_\alpha}] | \Phi_0 \rangle \\ &= -2D_{A_\beta} \delta_{A_\alpha A_\beta} \end{aligned}$$

Plugging the final forms of Term 1 (C2) and Term 2 (C3) in Eq. (19) we get

$$\begin{aligned} E_{AD-PQE} &= \langle \Phi_0 | \bar{H}_P | \Phi_0 \rangle + \sum_{A_\alpha} 2\theta_{A_\alpha}^2 D_{A_\alpha} \\ &\quad - \frac{1}{2} \sum_{A_\alpha, A_\beta} 2\theta_{A_\alpha} \theta_{A_\beta} D_{A_\beta} \delta_{A_\alpha A_\beta} \\ &= \langle \Phi_0 | \bar{H}_P | \Phi_0 \rangle + \sum_{A_\alpha} 2\theta_{A_\alpha}^2 D_{A_\alpha} - \sum_{A_\alpha} \theta_{A_\alpha}^2 D_{A_\alpha} \\ &\implies E_{AD-PQE} = \langle \Phi_0 | \hat{U}_P^\dagger \hat{H} \hat{U}_P | \Phi_0 \rangle + \sum_{A_\alpha} \theta_{A_\alpha}^2 D_{A_\alpha} \end{aligned} \quad (\text{C4})$$

which leads to Eq. (20) that we use for the energy evaluation during the post-optimization mapping.

REFERENCES:

- ¹W. Kohn, "Nobel lecture: Electronic structure of matter—wave functions and density functionals," *Reviews of Modern Physics* **71**, 1253 (1999).
- ²S. R. White, "Density matrix formulation for quantum renormalization groups," *Physical review letters* **69**, 2863 (1992).
- ³B. Huron, J. Malrieu, and P. Rancurel, "Iterative perturbation calculations of ground and excited state energies from multiconfigurational zeroth-order wavefunctions," *The Journal of Chemical Physics* **58**, 5745–5759 (1973).
- ⁴R. J. Buenker and S. D. Peyerimhoff, "Individualized configuration selection in ci calculations with subsequent energy extrapolation," *Theoretica chimica acta* **35**, 33–58 (1974).
- ⁵J. Čížek, "On the correlation problem in atomic and molecular systems. calculation of wavefunction components in ursell-type expansion using quantum-field theoretical methods," *J. Chem. Phys.* **45**, 4256–4266 (1966).
- ⁶J. Čížek, "On the use of the cluster expansion and the technique of diagrams in calculations of correlation effects in atoms and molecules," *Adv. Chem. Phys.* **14**, 35–89 (1969).
- ⁷J. Čížek and J. Paldus, "Correlation problems in atomic and molecular systems iii. rederivation of the coupled-pair many-electron theory using the traditional quantum chemical methods," *Int. J. Quantum Chem.* **5**, 359–379 (1971).
- ⁸R. J. Bartlett and M. Musiał, "Coupled-cluster theory in quantum chemistry," *Reviews of Modern Physics* **79**, 291 (2007).
- ⁹T. D. Crawford and H. F. Schaefer, "An introduction to coupled cluster theory for computational chemists," *Reviews in computational chemistry* **14**, 33–136 (2000).
- ¹⁰D. S. Abrams and S. Lloyd, "Simulation of many-body fermi systems on a universal quantum computer," *Physical Review Letters* **79**, 2586 (1997).
- ¹¹D. S. Abrams and S. Lloyd, "Quantum algorithm providing exponential speed increase for finding eigenvalues and eigenvectors," *Physical Review Letters* **83**, 5162 (1999).
- ¹²D. A. Lidar, I. L. Chuang, and K. B. Whaley, "Decoherence-free subspaces for quantum computation," *Physical Review Letters* **81**, 2594 (1998).
- ¹³D. P. DiVincenzo, "The physical implementation of quantum computation," *Fortschritte der Physik: Progress of Physics* **48**, 771–783 (2000).
- ¹⁴T. D. Ladd, F. Jelezko, R. Laflamme, Y. Nakamura, C. Monroe, and J. L. O'Brien, "Quantum computers," *nature* **464**, 45–53 (2010).
- ¹⁵A. Peruzzo, J. McClean, P. Shadbolt, M.-H. Yung, X.-Q. Zhou, P. J. Love, A. Aspuru-Guzik, and J. L. O'Brien, "A variational eigenvalue solver on a photonic quantum processor," *Nature communications* **5**, 4213 (2014).

¹⁶H. R. Grimsley, S. E. Economou, E. Barnes, and N. J. Mayhall, “An adaptive variational algorithm for exact molecular simulations on a quantum computer,” *Nature communications* **10**, 3007 (2019).

¹⁷A. Delgado, J. M. Arrazola, S. Jahangiri, Z. Niu, J. Izaac, C. Roberts, and N. Killoran, “Variational quantum algorithm for molecular geometry optimization,” *Physical Review A* **104**, 052402 (2021).

¹⁸D. Mondal, D. Halder, S. Halder, and R. Maitra, “Development of a compact Ansatz via operator commutativity screening: Digital quantum simulation of molecular systems,” *The Journal of Chemical Physics* **159**, 014105 (2023).

¹⁹C. Fenou, M. Hassan, D. Traoré, E. Giner, Y. Maday, and J.-P. Piquemal, “Overlap-adapt-vqe: practical quantum chemistry on quantum computers via overlap-guided compact ansätze,” *Communications Physics* **6**, 192 (2023).

²⁰L. Zhao, J. Goings, K. Shin, W. Kyoung, J. I. Fuks, J.-K. Kevin Rhee, Y. M. Rhee, K. Wright, J. Nguyen, J. Kim, *et al.*, “Orbital-optimized pair-correlated electron simulations on trapped-ion quantum computers,” *npj Quantum Information* **9**, 60 (2023).

²¹H. L. Tang, V. Shkolnikov, G. S. Barron, H. R. Grimsley, N. J. Mayhall, E. Barnes, and S. E. Economou, “qubit-adapt-vqe: An adaptive algorithm for constructing hardware-efficient ansätze on a quantum processor,” *PRX Quantum* **2**, 020310 (2021).

²²Y. S. Yordanov, V. Armaos, C. H. Barnes, and D. R. Arvidsson-Shukur, “Qubit-excitation-based adaptive variational quantum eigensolver,” *Communications Physics* **4**, 228 (2021).

²³M. Ostaszewski, E. Grant, and M. Benedetti, “Structure optimization for parameterized quantum circuits,” *Quantum* **5**, 391 (2021).

²⁴N. V. Tkachenko, J. Sud, Y. Zhang, S. Tretiak, P. M. Anisimov, A. T. Arrasmith, P. J. Coles, L. Cincio, and P. A. Dub, “Correlation-informed permutation of qubits for reducing ansatz depth in the variational quantum eigensolver,” *PRX Quantum* **2**, 020337 (2021).

²⁵F. Zhang, N. Gomes, Y. Yao, P. P. Orth, and T. Iadecola, “Adaptive variational quantum eigensolvers for highly excited states,” *Physical Review B* **104**, 075159 (2021).

²⁶S. Sim, J. Romero, J. F. Gonthier, and A. A. Kunitsa, “Adaptive pruning-based optimization of parameterized quantum circuits,” *Quantum Science and Technology* **6**, 025019 (2021).

²⁷S. Halder, A. Dey, C. Shrikhande, and R. Maitra, “Machine learning assisted construction of a shallow depth dynamic ansatz for noisy quantum hardware,” *Chem. Sci.* **15**, 3279–3289 (2024).

²⁸D. Halder, V. S. Prasanna, and R. Maitra, “Dual exponential coupled cluster theory: Unitary adaptation, implementation in the variational quantum eigensolver framework and pilot applications,” *The Journal of Chemical Physics* **157**, 174117 (2022).

²⁹D. Halder, S. Halder, D. Mondal, C. Patra, A. Chakraborty, and R. Maitra, “Corrections beyond coupled cluster singles and doubles through selected generalized rank-two operators: digital quantum simulation of strongly correlated systems,” *Journal of Chemical Sciences* **135**, 41 (2023).

³⁰D. Halder, D. Mondal, and R. Maitra, “Noise-independent Route towards the Genesis of a COMPACT Ansatz for Molecular Energetics: a Dynamic Approach,” *The Journal of Chemical Physics* **160**, XXXX (2024).

³¹N. H. Stair and F. A. Evangelista, “Simulating many-body systems with a projective quantum eigensolver,” *PRX Quantum* **2**, 030301 (2021).

³²S. Halder, C. Shrikhande, and R. Maitra, “Development of zero-noise extrapolated projective quantum algorithm for accurate evaluation of molecular energetics in noisy quantum devices,” *The Journal of Chemical Physics* **159** (2023).

³³J. P. Misiewicz and F. A. Evangelista, “Implementation of the projective quantum eigensolver on a quantum computer,” *arXiv preprint arXiv:2310.04520* (2023).

³⁴M. Cerezo, A. Sone, T. Volkoff, L. Cincio, and P. J. Coles, “Cost function dependent barren plateaus in shallow parametrized quantum circuits,” *Nature communications* **12**, 1791 (2021).

³⁵S. Wang, E. Fontana, M. Cerezo, K. Sharma, A. Sone, L. Cincio, and P. J. Coles, “Noise-induced barren plateaus in variational quantum algorithms,” *Nature communications* **12**, 6961 (2021).

³⁶F. A. Evangelista, G. K.-L. Chan, and G. E. Scuseria, “Exact parameterization of fermionic wave functions via unitary coupled cluster theory,” *The Journal of chemical physics* **151**, 244112 (2019).

³⁷Y. S. Yordanov, D. R. Arvidsson-Shukur, and C. H. Barnes, “Efficient quantum circuits for quantum computational chemistry,” *Physical Review A* **102**, 062612 (2020).

³⁸I. Magoulas and F. A. Evangelista, “Cnot-efficient circuits for arbitrary rank many-body fermionic and qubit excitations,” *Journal of Chemical Theory and Computation* **19**, 822–836 (2023).

³⁹H. Haken, “Generalized ginzburg-landau equations for phase transition-like phenomena in lasers, nonlinear optics, hydrodynamics and chemical reactions,” *Zeitschrift für Physik B Condensed Matter* **21**, 105–114 (1975).

⁴⁰H. Haken, *Synergetics: Introduction and advanced topics* (Springer Science & Business Media, 2013).

⁴¹A. Wunderlin and H. Haken, “Generalized ginzburg-landau equations, slaving principle and center manifold theorem,” *Zeitschrift für Physik B Condensed Matter* **44**, 135–141 (1981).

⁴²V. Agarawal, A. Chakraborty, and R. Maitra, “Stability analysis of a double similarity transformed coupled cluster theory,” *The Journal of Chemical Physics* **153**, 084113 (2020).

⁴³V. Agarawal, S. Roy, A. Chakraborty, and R. Maitra, “Accelerating coupled cluster calculations with nonlinear dynamics and supervised machine learning,” *The Journal of Chemical Physics* **154**, 044110 (2021).

⁴⁴V. Agarawal, C. Patra, and R. Maitra, “An approximate coupled cluster theory via nonlinear dynamics and synergetics: The adiabatic decoupling conditions,” *The Journal of Chemical Physics* **155**, 124115 (2021).

⁴⁵V. Agarawal, S. Roy, K. K. Shrawankar, M. Ghogale, S. Bharathi, A. Yadav, and R. Maitra, “A hybrid coupled cluster–machine learning algorithm: Development of various regression models and benchmark applications,” *The Journal of Chemical Physics* **156**, 014109 (2022).

⁴⁶C. Patra, V. Agarawal, D. Halder, A. Chakraborty, D. Mondal, S. Halder, and R. Maitra, “A synergistic approach towards optimization of coupled cluster amplitudes by exploiting dynamical hierarchy,” *ChemPhysChem* **24**, e202200633 (2023).

⁴⁷S. Halder, C. Patra, D. Mondal, and R. Maitra, “Machine learning aided dimensionality reduction toward a resource efficient projective quantum eigensolver: Formal development and pilot applications,” *The Journal of Chemical Physics* **158** (2023).

⁴⁸S. G. Mehendale, B. Peng, N. Govind, and Y. Alexeev, “Exploring parameter redundancy in the unitary coupled-cluster ansatz for hybrid variational quantum computing,” *The Journal of Physical Chemistry A* (2023).

⁴⁹P. V. S. Pathirage, J. T. Phillips, and K. D. Vogiatzis, “Exploration of the two-electron excitation space with data-driven coupled cluster,” *The Journal of Physical Chemistry A* (2024).

⁵⁰H. Haken and A. Wunderlin, “Slaving principle for stochastic differential equations with additive and multiplicative noise and for discrete noisy maps,” *Z. Phys. B* **47**, 179–187 (1982).

⁵¹H. Haken, “Application of the maximum information entropy principle to selforganizing systems,” *Zeitschrift für Physik B Condensed Matter* **61**, 335–338 (1985).

⁵²H. Haken, “Nonlinear equations. the slaving principle,” in *Advanced Synergetics* (Springer, 1983) pp. 187–221.

⁵³H. Haken, “Self-organization,” in *Synergetics* (Springer, 1983) pp. 191–227.

⁵⁴S. Wu, K. He, and Z. Huang, “Suppressing complexity via the slaving principle,” *Physical Review E* **62**, 4417 (2000).

⁵⁵W. Iskra, M. Müller, and I. Rotter, “Self-organization in the nuclear system: I. the slaving principle,” *Journal of Physics G: Nuclear and Particle Physics* **19**, 2045 (1993).

⁵⁶Z. Zheng, C. Xu, J. Fan, M. Liu, and X. Chen, “Order parameter

dynamics in complex systems: From models to data," *Chaos: An Interdisciplinary Journal of Nonlinear Science* **34** (2024).

⁵⁷K. Kowalski, "Properties of coupled-cluster equations originating in excitation sub-algebras," *The Journal of Chemical Physics* **148**, 094104 (2018).

⁵⁸N. P. Bauman, E. J. Bylaska, S. Krishnamoorthy, G. H. Low, N. Wiebe, C. E. Granade, M. Roetteler, M. Troyer, and K. Kowalski, "Downfolding of many-body hamiltonians using active-space models: Extension of the sub-system embedding sub-algebras approach to unitary coupled cluster formalisms," *The Journal of Chemical Physics* **151**, 014107 (2019).

⁵⁹K. Kowalski, "Dimensionality reduction of the many-body problem using coupled-cluster subsystem flow equations: Classical and quantum computing perspective," *Physical Review A* **104**, 032804 (2021).

⁶⁰N. P. Bauman and K. Kowalski, "Coupled cluster downfolding theory: Towards universal many-body algorithms for dimensionality reduction of composite quantum systems in chemistry and materials science," *Materials Theory* **6**, 1–19 (2022).

⁶¹K. Kowalski and N. P. Bauman, "Quantum flow algorithms for simulating many-body systems on quantum computers," *Physical Review Letters* **131**, 200601 (2023).

⁶²S. H. Strogatz, *Nonlinear dynamics and chaos: with applications to physics, biology, chemistry, and engineering* (CRC press, 2018).

⁶³P. Szakács and P. R. Surján, "Stability conditions for the coupled cluster equations," *Int. J. Quantum Chem.* **108**, 2043–2052 (2008).

⁶⁴H. Haken and M. Synergetics, "Introduction and advanced topics," *Physics and Astronomy Online Library* , 758 (2004).

⁶⁵N. G. Van Kampen, "Elimination of fast variables," *Physics Reports* **124**, 69–160 (1985).

⁶⁶J. Romero, R. Babbush, J. R. McClean, C. Hempel, P. J. Love, and A. Aspuru-Guzik, "Strategies for quantum computing molecular energies using the unitary coupled cluster ansatz," *Quantum Science and Technology* **4**, 014008 (2018).

⁶⁷Y. Cao, J. Romero, J. P. Olson, M. Degroote, P. D. Johnson, M. Kieferová, I. D. Kivlichan, T. Menke, B. Peropadre, N. P. Sawaya, *et al.*, "Quantum chemistry in the age of quantum computing," *Chemical reviews* **119**, 10856–10915 (2019).

⁶⁸D. Gottesman, "An introduction to quantum error correction and fault-tolerant quantum computation," in *Quantum information science and its contributions to mathematics, Proceedings of Symposia in Applied Mathematics*, Vol. 68 (2010) pp. 13–58.

⁶⁹B. M. Terhal, "Quantum error correction for quantum memories," *Reviews of Modern Physics* **87**, 307 (2015).

⁷⁰Z. Cai, R. Babbush, S. C. Benjamin, S. Endo, W. J. Huggins, Y. Li, J. R. McClean, and T. E. OâĂŹBrien, "Quantum error mitigation," *Reviews of Modern Physics* **95**, 045005 (2023).

⁷¹K. Temme, S. Bravyi, and J. M. Gambetta, "Error mitigation for short-depth quantum circuits," *Physical review letters* **119**, 180509 (2017).

⁷²T. Giurgica-Tiron, Y. Hindy, R. LaRose, A. Mari, and W. J. Zeng, "Digital zero noise extrapolation for quantum error mitigation," in *2020 IEEE International Conference on Quantum Computing and Engineering (QCE)* (IEEE, 2020) pp. 306–316.

⁷³Y. Kim, C. J. Wood, T. J. Yoder, S. T. Merkel, J. M. Gambetta, K. Temme, and A. Kandala, "Scalable error mitigation for noisy quantum circuits produces competitive expectation values," *Nature Physics* , 1–8 (2023).

⁷⁴Z. Cai, "A practical framework for quantum error mitigation," *arXiv preprint arXiv:2110.05389* (2021).

⁷⁵R. Takagi, S. Endo, S. Minagawa, and M. Gu, "Fundamental limits of quantum error mitigation," *npj Quantum Information* **8**, 114 (2022).

⁷⁶H. Abraham *et. al.*, "Qiskit: An open-source framework for quantum computing," (2021).

⁷⁷Q. Sun, T. C. Berkelbach, N. S. Blunt, G. H. Booth, S. Guo, Z. Li, J. Liu, J. D. McClain, E. R. Sayfutyarova, S. Sharma, *et al.*, "Pyscf: the python-based simulations of chemistry framework," *Wiley Interdisciplinary Reviews: Computational Molecular Science* **8**, e1340 (2018).

⁷⁸R. LaRose, A. Mari, S. Kaiser, P. J. Karalekas, A. A. Alves, P. Czarnik, M. E. Mandouh, M. H. Gordon, Y. Hindy, A. Robertson, P. Thakre, M. Wahl, D. Samuel, R. Mistri, M. Tremblay, N. Gardner, N. T. Stemen, N. Shammah, and W. J. Zeng, "Mitiq: A software package for error mitigation on noisy quantum computers," *Quantum* **6**, 774 (2022).

⁷⁹H. Haken, "Discrete dynamics of complex systems," *Discrete Dynamics in Nature and Society* **1**, 1–8 (1997).